The Journal of Immunology

4E-BP–Dependent Translational Control of *Irf8* Mediates Adipose Tissue Macrophage Inflammatory Response

Dana Pearl, Sakie Katsumura, Mehdi Amiri, Negar Tabatabaei, Xu Zhang, Valerie Vinette, Xinhe Pang, Shawn T. Beug, Sung-Hoon Kim, Laura M. Jones, Nathaniel Robichaud, Sang-Ging Ong, Jian-Jun Jia, Hamza Ali, Michel L. Tremblay, Maritza Jaramillo, Tommy Alain, Masahiro Morita, Nahum Sonenberg and Soroush Tahmasebi

J Immunol 2020; 204:2392-2400; Prepublished online 25 March 2020;
doi: 10.4049/jimmunol.1900538
http://www.jimmunol.org/content/204/9/2392

The Journal of Immunology is published twice each month by
The American Association of Immunologists, Inc.,
1451 Rockville Pike, Suite 650, Rockville, MD 20852

Print ISSN: 0022-1767 Online ISSN: 1550-6606.

4E-BP–Dependent Translational Control of *Irf8* Mediates Adipose Tissue Macrophage Inflammatory Response

Dana Pearl,[*,†,1] Sakie Katsumura,[‡,§,1] Mehdi Amiri,[*,†] Negar Tabatabaei,[¶] Xu Zhang,[*,†] Valerie Vinette,[*,†] Xinhe Pang,[¶] Shawn T. Beug,[‖,#] Sung-Hoon Kim,[*,†] Laura M. Jones,[*,†] Nathaniel Robichaud,[*,†] Sang-Ging Ong,[¶,] Jian-Jun Jia,[‖,#] Hamza Ali,[‖,#] Michel L. Tremblay,[*,†] Maritza Jaramillo,[††] Tommy Alain,[‖,#] Masahiro Morita,[‡,§,‡‡] Nahum Sonenberg,[*,†] and Soroush Tahmasebi[¶]**

Deregulation of mRNA translation engenders many human disorders, including obesity, neurodegenerative diseases, and cancer, and is associated with pathogen infections. The role of eIF4E-dependent translational control in macrophage inflammatory responses in vivo is largely unexplored. In this study, we investigated the involvement of the translation inhibitors eIF4E-binding proteins (4E-BPs) in the regulation of macrophage inflammatory responses in vitro and in vivo. We show that the lack of 4E-BPs exacerbates inflammatory polarization of bone marrow–derived macrophages and that 4E-BP–null adipose tissue macrophages display enhanced inflammatory gene expression following exposure to a high-fat diet (HFD). The exaggerated inflammatory response in HFD-fed 4E-BP–null mice coincides with significantly higher weight gain, higher *Irf8* mRNA translation, and increased expression of IRF8 in adipose tissue compared with wild-type mice. Thus, 4E-BP–dependent translational control limits, in part, the proinflammatory response during HFD. These data underscore the activity of the 4E-BP–IRF8 axis as a paramount regulatory mechanism of proinflammatory responses in adipose tissue macrophages. ***The Journal of Immunology*****, 2020, 204: 2392–2400.**

The plastic nature of adaptive and innate immune responses relies on a rapid readjustment of gene expression (1). mRNA translational control allows for swift changes in the proteome, which is required for a prompt immune response, and precedes alterations in transcription to secure a long-lasting effect (2, 3). Translation is divided into three steps: initiation, elongation, and termination. Translation initiation is the process by which the ribosome is recruited to the mRNA and scans the 5′ untranslated region to locate the start codon (4). All nuclear-encoded mRNAs harbor the structure m^7GpppN (where m is a methyl group and N is any nucleotide) known as "cap" at their 5′ ends. The cap is bound by the cap-binding protein eukaryotic translation initiation factor 4E (eIF4E) in a complex with the scaffolding protein eIF4G and an RNA helicase eIF4A, termed eIF4F. The interaction of eIF4F with the 43S preinitiation complex (consisting of the initiator $tRNA^{Met}$, eIF1, 1A, 2, and 3 and the 40S small ribosomal subunit) places the ribosome in the vicinity of the cap to start scanning (4). Members of a family of small proteins (∼15–20 kDa), known as eIF4E-binding proteins (4E-BPs; there are three paralogs in mammals, 4E-BP1, 2, and 3), compete with eIF4G for eIF4E binding and block the assembly of the eIF4F complex. 4E-BPs, when dephosphorylated, exhibit a high affinity for eIF4E, impede eIF4E binding to eIF4G, and, consequently, block translation initiation (5). The serine/threonine kinase complex

*Rosalind and Morris Goodman Cancer Research Center, McGill University, Montreal, Quebec H3A 1A3, Canada; [†]Department of Biochemistry, McGill University, Montreal, Quebec H3A 1A3, Canada; [‡]Department of Molecular Medicine, University of Texas Health Science Center at San Antonio, San Antonio, TX 78229; [§]Barshop Institute for Longevity and Aging Studies, University of Texas Health Science Center at San Antonio, San Antonio, TX 78229; [¶]Department of Pharmacology, University of Illinois at Chicago, Chicago, IL 60612; [‖]Children's Hospital of Eastern Ontario Research Institute, Ottawa, Ontario K1H 8L1, Canada; [#]Department of Biochemistry, Microbiology and Immunology, University of Ottawa, Ottawa, Ontario K1H 8M5, Canada; **Division of Cardiology, Department of Medicine, University of Illinois College of Medicine, Chicago, IL 60612; [††]Institut National de la Recherche Scientifique–Institut Armand-Frappier, Laval, Quebec H7V 1B7, Canada; and [‡‡]Institute of Resource Development and Analysis, Kumamoto University, Kumamoto 860-0811, Japan

[1]D.P. and S.K. contributed equally to this work.

ORCIDs: 0000-0002-7742-5918 (X.P.); 0000-0002-9991-3306 (S.T.B.); 0000-0002-3825-5653 (S.-H.K.); 0000-0002-7653-0767 (N.R.); 0000-0002-5029-8138 (J.-J.J.); 0000-0002-6215-5409 (H.A.); 0000-0002-0281-541X (M.L.T.); 0000-0002-1910-5684 (M.J.); 0000-0002-0396-9138 (T.A.); 0000-0002-8627-084X (M.M.); 0000-0002-4707-8759 (N.S.).

Received for publication May 10, 2019. Accepted for publication February 2, 2020.

This work was supported by a Uehara Memorial Foundation Postdoctoral Fellowship (to S.K.). M.M. is a recipient of a University of Texas Rising Stars Award, McDermott Start-up Funding, a Helen F. Kerr Foundation Grant, and a Grant-in-Aid for Scientific Research (18K07237). This work was also supported by an Israel-Canada International Development Research Centre grant (to M.L.T.).

D.P., M.M., S.T., and N.S. designed research; D.P., S.K., M.A., N.T., V.V., S.T.B., S.-H.K., L.M.J., J.-J.J., H.A., M.M., S.T., X.P., S.-G.O., X.Z., and N.R. performed research; T.A. and M.L.T. contributed reagents and analytic tools; D.P., M.A., V.V., S.T.B., S.K., L.M.J., J.-J.J., H.A., T.A., M.M., S.T., N.S., and M.J. analyzed research and edited manuscript; and D.P., S.T., and N.S. wrote the manuscript.

Address correspondence and reprint requests to Dr. Masahiro Morita, Prof. Nahum Sonenberg, or Dr. Soroush Tahmasebi, Department of Molecular Medicine, University of Texas Health Science Center at San Antonio, South Texas Research Facility, MC 8257, 7703 Floyd Curl Drive, San Antonio, TX 78229-3900 (M.M.); Rosalind and Morris Goodman Cancer Centre, Life Sciences Complex, 1160 Pine Avenue West, Montreal, QC H3A 1A3, Canada (N.S.); or Department of Pharmacology, College of Medicine, University of Illinois at Chicago, MC868, 835 S Wolcott Avenue E403, Chicago, IL 60612 (S.T.). E-mail addresses: moritam@uthscsa.edu (M.M.), or nahum.sonenberg@mcgill.ca (N.S.), or sorousht@uic.edu (S.T.)

The online version of this article contains supplemental material.

Abbreviations used in this article: BMDM, bone marrow–derived macrophage; CLS, crown-like structure; DKO, double knockout; 4E-BP, eIF4E-binding protein; eIF4E, eukaryotic translation initiation factor 4E; eWAT, epididymal white adipose tissue; HFD, high-fat diet; IHC, immunohistochemical/immunohistochemistry; IRF, IFN regulatory factor; Mϕ, macrophage; mTORC1, mammalian/mechanistic target of rapamycin complex 1; RER, respiratory exchange ratio; RT-qPCR, real-time quantitative PCR; TKO, triple knockout; WT, wild-type.

mammalian/mechanistic target of rapamycin complex 1 (mTORC1) impairs the activity of the 4E-BPs through the phosphorylation of residues surrounding their eIF4E-binding motif, abrogating their eIF4E-binding function (6).

4E-BP–dependent control of translation plays a key role in the regulation of innate immunity (1). Mice lacking 4E-BP1 and 4E-BP2 are resistant to vesicular stomatitis virus infection via enhanced type I IFN response (7). Similarly, enhanced type I IFN response renders 4E-BP1/2 double knockout (DKO) mice resistant to *Leishmania major* infection (8). Notably, bone marrow–derived macrophages (BMDMs) from DKO mice infected with *L. major* exhibit a significant reduction (~45%) in parasite load compared with wild-type (WT) counterparts (8).

4E-BP–dependent translational control also plays a critical role in metabolism and metabolic disorders (9). 4E-BP1, 4E-BP2, and 4E-BP3 are highly expressed in metabolic tissues, such as adipose, liver, pancreas, and muscle tissues (10, 11). 4E-BP1/2 DKO mice gain significantly more weight when fed a high-fat diet (HFD) and are less sensitive to insulin compared with WT mice (12, 13). Consistent with these findings, skeletal muscle–specific overexpression of a constitutively active 4E-BP1 (T37A. T46A) preserves insulin sensitivity, improves glucose clearance rate, and decreases basal glucose levels in response to an HFD (14).

Despite the importance of 4E-BP–dependent translational control in many physiological and pathological conditions, our knowledge of the specific cell types that mediate these effects is limited. Among the various immune cell types, macrophages (Mϕs) in particular play an important role in both innate immune responses and metabolic disorders. Mϕs are the first responders to invading pathogens, yet in addition to their central role in innate immunity, they play a critical role in normal tissue homeostasis (15, 16). They are broadly categorized into two functional groups: pro- and anti-inflammatory phenotypes (17). Inflammatory triggers, such as LPS, an HFD, or tissue damage, promote infiltration and polarization of inflammatory Mϕs in target tissues (18).

Recent studies using 4E-BP1/2 DKO BMDMs indicate that 4E-BPs limit both anti-inflammatory and inflammatory responses in vitro (19, 20). However, the role of 4E-BPs in the regulation of Mϕ-proinflammatory responses in vivo and the translational targets of 4E-BPs that mediate this effect remained unexplored. To address this, we generated 4E-BP1/2/3 triple knockout (TKO) mice and studied the inflammatory response in vitro using BMDMs challenged with LPS/IFN-γ and in vivo using animals fed with HFD. Strikingly, we found that TKO BMDMs and white adipose tissue resident Mϕs have a higher propensity than WT to polarize into a proinflammatory state. The increase in proinflammatory gene expression is mediated by the translational upregulation of IFN regulatory factor (IRF) 8, a key transcriptional factor involved in Mϕ maturation and inflammatory response (21). Our data highlight the importance of 4E-BP–dependent translational control of *Irf8* in controlling Mϕ polarization and inflammatory response.

Materials and Methods

Mice

The McGill University Animal Resource Centre committee approved all experiments. 4E-BP1/2/3 TKO mice were generated by crossing the previously described C57BL/6 4E-BP1/2 DKO mice (12) with 4E-BP3 knockout mice (KO-4974 [Eif4ebp3tm1.1(KOMP)Vlcg]) from The Knockout Mouse Project Repository at University of California, Davis. Congenic C57BL/6 4E-BP1/2/3 TKO mice were obtained by backcrossing the TKO strain for 10 generations to inbred WT C57BL/6 mice from The Jackson Laboratory. Animals were maintained in the animal facility at the Goodman Cancer Research Centre at McGill University under standard conditions. After 10 generations of the backcross, WT and TKO mice have been maintained separately. Our mice are kept together in the same room and the same rack and have not been relocated. Thus, the mice experienced the same light-dark cycle, temperature, humidity, water treatment, and many other environmental factors that may impact the microbiome. Six-week-old male mice were fed either a normal diet (2020×; 24% protein, 60% carbohydrate, and 16% fat; Envigo) or an HFD (D12492; 20% protein, 20% carbohydrate, and 60% fat; Research Diets) up to 16 wk of age and weighed every week. Then, mice were used for metabolic experiments and then sacrificed using CO_2 euthanasia or rodent mixture i.p. injection (ketamine and xylene), and tissues were excised, weighed, and used or frozen in liquid nitrogen for further use. Mice were handled by the same animal technician, and handling time was identical between groups. All the experiments have been performed on age- and sex-matched animals; thus, the change in microbiome composition resulting from aging or gender does not influence our results.

Abs

The primary Abs against mouse are as follows: IRF-1, 4E-BP1, 4E-BP2, T37/46–phosphorylated 4E-BP1, S240/244–phosphorylated rpS6, and β-actin were purchased from Cell Signaling Technology. Abs against mouse rpS6 and IRF-8 were purchased from Santa Cruz Biotechnology.

Metabolic cages: locomotion and VO_2 measurement

Five representative mice from each group were placed in individual Oxymax/Comprehensive Lab Animal Monitoring System (Columbus Instruments) metabolic cages at the end of the metabolic study for calorimetric and locomotor assessment. The mice were acclimatized to the cages for 3 d and then continuous measurements were recorded for 24 h (one full light-dark cycle) at 25˚C with food and water available ad libitum. Oxygen consumption and locomotor activity were analyzed during the 24 h time period according to the manufacturer's protocol (Columbus Instruments). Oxygen consumption is expressed as the volume of O_2 consumed per kilogram of body weight per hour (ml/kg/h). Respiratory exchange ratio (RER) is calculated as the ratio between carbon dioxide production and oxygen consumption (RER = VCO_2/VO_2) and is used to determine macromolecule metabolism. Values fall between 0.7 and 1, with 0.7 representing 100% of O_2 consumed by fat and 1 representing 100% of O_2 consumed by carbohydrates. Locomotor activity is measured as bouts per minute.

Histology, immunohistochemistry, quantification

Paraffin-embedded tissues were sectioned at 4 μm and stained with H&E. The slides were scanned using the Aperio Scanscope. For immunohistochemical (IHC) analysis, liver tissue and epididymal white adipose tissue (eWAT) were fixed with zinc-fixative (BD Biosciences) for 36 h and then paraffin-embedded and sectioned. For IHC analysis of the Mϕ marker F4/80, the sections were blocked for 5 min using POWERBLOCK blocking reagent (BioGenex) and incubated with primary anti-mouse F4/80 (Santa Cruz Biotechnology) overnight at 4˚C. The samples were incubated with ImmPRESS HRP anti-rat IgG (Peroxidase) (Vector Laboratories) for 1 h and exposed to 3,3′-diaminobenzidine (DAB) staining for 3 min (liver) or 30 s (adipose tissue). $F4/80^+$ cells were quantified using the DL_IHC Ki67 algorithm (Spectrum Analysis software) on five randomly selected 0.8-mm^2 sections per slide ($n = 3$). Crown-like structures (CLS) were quantified by counting $F4/80^+$ cells surrounding adipocytes in five randomly selected 0.8-mm^2 sections per slide ($n = 3$). A mouse monoclonal IRF-8 Ab from Santa Cruz Biotechnology (E-9) was used for IHC analysis of eWATs.

Bone marrow isolation and culture in vitro

Mice were euthanized, and the cleaned tibias and femurs were excised and placed in a petri dish with Mϕ media (DMEM-high glucose, 10% heat-inactivated FBS, 1% L-glutamine, 1% sodium pyruvate, 1% penicillin-streptomycin, 1% nonessential amino acids, 0.5% 2-ME). In sterile conditions, the bones were cut in half, placed with the cut-half facing downward in a microtube tube with 500 μl of Mϕ media, and centrifuged at max speed (21,000 × *g*) for 5 s. The bones were then placed into another microtube with 500 μl of Mϕ media. The pellet was resuspended, and the supernatant was collected. This process was repeated twice to ensure all bone marrow was collected from the bones. The bone marrow–cell suspension was then filtered through a 40-μm cell strainer and centrifuged at 1200 rpm for 5 min at 4˚C. The cells were seeded at a density of 5 million cells per 10 cm^2 petri dish with 8 ml of Mϕ media supplemented with 30 ng/ml of M-CSF (PeproTech). The cells were kept at 37˚C in a 5% CO_2 incubator, and M-CSF was replenished every 3 d. On day 8, the cells were replated into 12-well plates with fresh M-CSF. On day 10, the cells were stimulated with LPS (100 ng/ml; Sigma-Aldrich) and IFN-γ (20 ng/ml) for 24 h at

37°C. After 24 h, the cells and media were collected for real-time quantitative PCR (RT-qPCR), Western blot, and ELISA analysis.

Lentiviral production and transduction into BMDMs

The 293FT cells (Invitrogen) were cultured in DMEM/10% (vol/vol) FBS medium with 400 μg/ml neomycin (BioShop) according to the manufacturer's instructions. Eight hours before transfection, the medium was replaced by antibiotic-free medium. Using Lipofectamine 2000, 10 μg of the doxycycline-inducible 4E-BP1–4ala plasmid, 6.5 μg of psPAX2, and 3.5 μg of pMD2.G packaging plasmids were used to transfect 8×10^6 293FT cells in a 10 cm^2 dish, as described by Tahmasebi et al. (22). The medium was collected and replaced for 3 d and then pooled and centrifuged in an SW32-Ti Rotor (Beckman Coulter) at 25,000 rpm for 1.5 h. The viral pellet was resuspended in DMEM and 10% (vol/vol) heat-inactivated FBS and was rotated overnight at 4°C. The resulting concentrated virus solution was used to infect the TKO BMDMs for 48 h on day 8 in culture with Polybrene (6 μg/ml). The BMDMs were then selected using puromycin (5 μg/ml) for 24 h and then stimulated with LPS and IFN-γ or vehicle in the presence or absence of doxycycline (1 μg/ml).

Purification of immune cells

Lymphocytes were magnetically isolated from the spleen and lymph nodes from a 5-wk-old female using the kits from STEMCELL Technologies. The samples were negatively selected for B cells and $CD4^+$ and $CD8^+$ T cells, and positively selected for $CD4^+$ $CD25^+$ T regulatory cells.

Human Mϕ generation and polarization

Blood was collected from healthy donors, and PBMCs were acquired by density gradient centrifugation at 1600 rpm for 45 min (Lymphoprep; Alere Technologies). PBMCs were counted, resuspended in Isove modified DMEM media (Wisent), and seeded at a concentration of 4×10^6 cells per milliliter into 12-well polystyrene plates (Corning). The plates were kept at 37°C in a 5% CO_2 incubator for 3 h to facilitate the adherence of monocyte to the plate surface. Nonadherent cells were washed off with Isove modified DMEM media. To generate Mϕs, adherent cells were cultured for 7 d in a complete media (Isove modified DMEM, 10% heat-inactivated FBS, 1% penicillin-streptomycin) with 10 ng/ml of recombinant human M-CSF (R&D Systems). On the third day of incubation, cells were washed, and fresh complete media with M-CSF was added. On day 8, cells were washed once again, and complete media supplemented with either IFN-γ (20 ng/ml; Invitrogen) to generate inflammatory Mϕs or IL-4 (20 ng/ml; R&D Systems) to generate anti-inflammatory Mϕs was added. The stimulated cells were kept at 37°C in a 5% CO_2 incubator for 2 d and then harvested.

Polysome-profiling analysis

Polysome profile analysis was carried out as previously described (23). Briefly, frozen mouse livers were homogenized in 425 μl of hypotonic buffer (5 mM Tris-HCl [pH 7.5], 2.5 mM $MgCl_2$, 1.5 mM KCl, 1×-protease inhibitor mixture [EDTA-free]) with 100 μg/ml cycloheximide, 2 mM DTT, and 100 U of RNasin with a glass homogenizer. The lysates were transferred to 1.5-ml microtubes and then 0.5% Triton X-100 and 0.5% sodium deoxycholate were added. Lysates were precleared by centrifugation at 21,000 × *g* for 5 min at 4°C and the OD260 nm for each sample was measured to determine yield using NanoDrop. Equal amounts of each sample were loaded (OD 260 nm 10–30) onto sucrose gradients with 10% of the samples kept as inputs. The samples were sedimented by velocity centrifugation at 36,000 × *g* for 2 h at 4°C using an SW40Ti Rotor in a Beckman Coulter ultracentrifuge. Chasing solution (60% [w/v] sucrose/water with bromophenol blue) was run through the gradient at 1.5 ml/min, A254 nm was measured, and fractions were collected every 35 s for RNA analysis.

RNA isolation, RT-PCR, and RT-qPCR analyses

RNA was isolated from tissues and primary cells using TRIzol (Invitrogen) following the manufacturer's instructions. The cDNA (1 μg) was made using Invitrogen SuperScript II Reverse Transcriptase. PCRs were carried out using Titanium Taq Polymerase (Clontech Laboratories) or AccuStart II PCR SuperMix (Quantabio). RT-qPCRs were carried out using iQ SYBR Green Supermix (Bio-Rad Laboratories, Hercules, CA) according to the manufacturer's instructions. Primers are listed in Supplemental Table I.

BioGPS database analysis

Murine expression data for the three genes, eIF4EBP-1, 2, and 3, were collected from the BioGPS database (http://biogps.org/#goto=genereport&id=13685,13688,108112). The means and SDs of the indicated immune cell populations were calculated and graphed in Excel.

Statistical analysis

Statistical analysis was conducted using Prism 7 software. Each figure indicates which statistical test was performed of either unpaired Student *t* test, one-way ANOVA, or two-way ANOVA with Bonferroni post hoc test. Any p values < 0.05 are considered statistically significant.

Results

Lack of 4E-BPs promotes inflammatory polarization of BMDMs

The BioGPS database shows that mRNAs for the three 4E-BP paralogs are expressed in various immune cells, including Mϕs (Supplemental Fig. 1A). We quantified the amounts of *4E-BP1*, *2*, and *3* mRNAs in different mouse and human immune cells via RT-qPCR (Supplemental Fig. 1B) and Western blot analysis for 4E-BP1 and 2 (Supplemental Fig. 1C; we failed to obtain a good-quality Ab against 4E-BP3). In accordance with the gene expression data in the BioGPS database, all three 4E-BP paralogs were expressed in mouse and human Mϕs. Polarization of Mϕs toward inflammatory or anti-inflammatory phenotypes induces expression of 4E-BPs to various extents (Supplemental Fig. 1A, 1B). To address the role of 4E-BPs in Mϕ-proinflammatory responses, we generated 4E-BP1/2/3 TKO mice (*Materials and Methods*, Supplemental Fig. 2A–C). BMDMs from WT and TKO mice were stimulated with LPS and IFN-γ for 24 h. As expected, LPS/IFN-γ stimulation of BMDMs resulted in activation of mTORC1 signaling as evidenced by increased phosphorylation of ribosomal protein S6 (24) (Fig. 1A). Although the lack of 4E-BPs did not affect Mϕ differentiation, as quantified by the percentage of $F4/80^+CD11b^+$ cells (Supplemental Fig. 1D), the lack of 4E-BPs resulted in enhanced production of the proinflammatory cytokines, IL-6 (fold change: 1.2 TKO versus WT), IL-12b (1.6 TKO versus WT), TNF-α (1.2 in TKO versus WT), and IFN-β (6.5 in TKO versus WT) (Fig. 1B). Consistent with the ELISA results, TKO BMDMs stimulated with LPS/IFN-γ expressed significantly higher levels of mRNAs encoding proinflammatory proteins, such as *IL-12b*, *TNFα*, *Nos2*, *Ccr7*, *Ptgs2*, and *Cxcl11*, than their WT counterparts (Fig. 1C). Similar results were obtained when BMDMs were stimulated for shorter (3 or 6 h) time periods (Supplemental Fig. 2D–G). Importantly, expression of a phosphorylation-resistant 4E-BP1, which constitutively inhibits eIF4E (4E-BP1–4ala) (25) in TKO BMDMs decreased the production of proinflammatory cytokines (Supplemental Fig. 2H), thus partially reversing the proinflammatory phenotype seen in the absence of 4E-BPs. These data demonstrate that 4E-BPs play a critical role in regulating inflammatory responses in Mϕs.

TKO mice are prone to HFD-induced obesity and exhibit increased accumulation of inflammatory Mϕs in adipose tissue

Obesity is strongly associated with chronic low-grade inflammation in which adipose tissue Mϕs polarize toward an inflammatory state and secrete proinflammatory cytokines (18). Inflammatory Mϕs phagocytize debris from necrotic adipocytes and secrete cytokines to maintain a proinflammatory milieu (26), resulting in chronic inflammation and metabolic disorder (18, 27, 28). Thus, HFD-induced obesity serves as a useful model to examine Mϕ polarization in vivo. To study the role of 4E-BPs in Mϕ polarization in response to diet-induced obesity, we subjected 6-wk-old male TKO and WT mice to normal diet or HFD up to 16 wk. After the first week of HFD, the WT and TKO mouse weights began to diverge (Fig. 2A), and after 10 wk, the TKO mice gained significantly more weight (~20%) than their WT counterparts (Fig. 2A–C). No significant differences in weight gain were observed between WT and TKO mice receiving normal diet (Fig. 2C, Supplemental Fig. 3A). The excessive weight gain seen in TKO HFD mice cannot be attributed

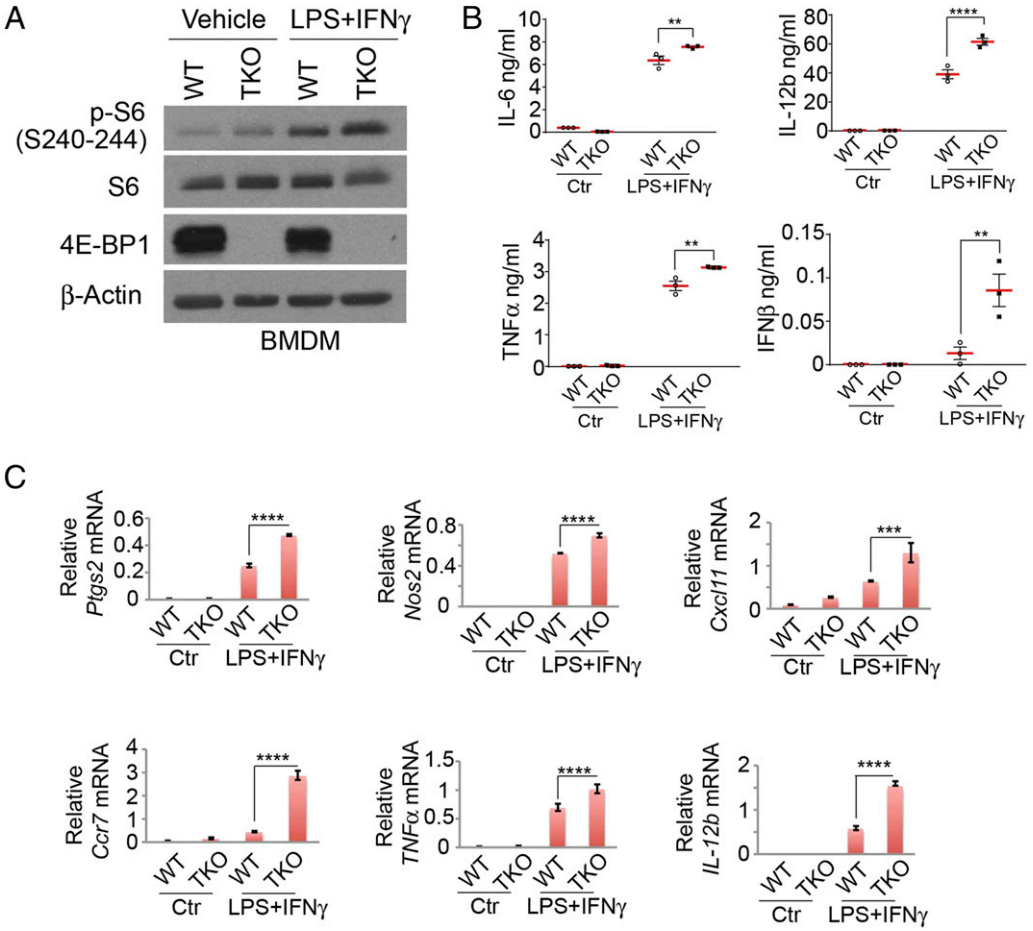

FIGURE 1. 4E-BPs play a key role in proinflammatory Mϕ polarization. (**A**) Western blot analysis of WT and TKO BMDMs stimulated with LPS (100 ng/ml) and IFN-γ (20 ng/ml) or vehicle. (**B**) Analysis of cytokine secretions of WT and TKO BMDMs by ELISA 24 h after treatment with LPS (100 ng/ml) and IFN-γ (20 ng/ml) or vehicle. $^{**}p < 0.01$, $^{****}p < 0.0001$. Two-way ANOVA with Bonferroni post hoc test ($n = 3$). (**C**) RT-qPCR analysis of proinflammatory genes in WT and TKO BMDMs stimulated with either vehicle (sterile water) or LPS (100 ng/ml) and IFN-γ (20 ng/ml) for 24 h. Data were normalized to the housekeeping gene Hprt. Results are presented as a mean ± SD ($n = 3$). $^{***}p < 0.001$, $^{****}p < 0.0001$. A representative experiment of two independent experiments (each carried out in triplicate) is presented.

to higher food consumption or decreased movement, as they were similar between WT and TKO mice (Supplemental Fig. 3B–E). However, measurement of the oxygen consumption rate and the RER showed reduced metabolism in TKO HFD mice (Fig. 2D, Supplemental Fig. 3D). TKO mice fed an HFD had significantly heavier livers, brown adipose tissue, pancreases, kidneys, and spleens (Fig. 2E). In contrast, no difference was observed in tissue weight or metabolic parameters of WT and TKO mice fed a normal diet (Fig. 2E, Supplemental Fig. 3F).

Although we found no significant difference in eWAT weight (Fig. 2E) and adipocyte size (Supplemental Fig. 4A, 4B) between HFD-fed WT and TKO mice, the number of F4/80$^+$ CLS (indicative of inflammatory Mϕ polarization) (26) significantly increased in HFD-fed TKO mice compared with WT mice (mean: 19.1 in WT HFD versus 43.7 in TKO HFD) (Fig. 3A, 3B, bottom panel). These data suggest that increased accumulation of inflammatory Mϕs in TKO eWAT is independent of adipocyte size.

Next, we sought to examine the translation control mechanism that leads to the inflammatory phenotype in TKO Mϕs. eIF4E-dependent translation plays a key role in the regulation of innate immunity through translation control of IRFs (1, 7, 29). Notably, the activity of eIF4E has been linked to the translation of *Irf8* mRNA and inflammatory Mϕ polarization (29). We also observed that transcription of *Il12b* and *Nos2*, two known IRF8 targets (29), are highly increased in TKO BMDMs in response to LPS/IFN-γ treatment (Fig. 1C, Supplemental Fig. 2D, 2F). Consequently, we hypothesized that the increase in translation of *Irf8* as a result of the absence of 4E-BPs plays a central role in the inflammatory phenotype observed in eWAT Mϕs. We first examined IRF8 protein and mRNA levels in WT and TKO eWAT. On a normal diet, the protein and mRNA levels of IRF8 did not significantly differ between WT and TKO mice (Fig. 3C). However, on an HFD, IRF8 protein increased significantly (relative IRF8 protein levels [mean]: 0.99 in WT versus 4.2 in TKO) in TKO eWAT as compared with WT counterparts, whereas mRNA levels were similar in the two groups (Fig. 3C). IRF8 immunostaining of the eWAT demonstrated that expression of IRF8 significantly increased in the CLS in HFD-fed TKO mice compared with WT mice (Fig. 3D). In addition, expression of proinflammatory genes (including IRF8 targets *Il12-b* and *Nos2*) significantly increased in TKO F480$^+$Cd11b$^+$ eWAT Mϕs as compared with WT cells (Fig. 3E). In support of this finding, expression of IRF8 was also significantly induced in TKO BMDMs in response to LPS/IFN-γ treatment compared with WT BMDMs (Supplemental Fig. 4C, left panel) and shRNA-mediated suppression of IRF8 expression in TKO cells partially alleviated proinflammatory phenotypes of these cells (Supplemental Fig. 4D). IRF8 and IRF1 are known to coregulate transcription of proinflammatory factors in Mϕs (21). In addition, recent studies highlighted the importance of several IRFs (such as IRF1, IRF3, IRF4, IRF5, and IRF7) in obesity and

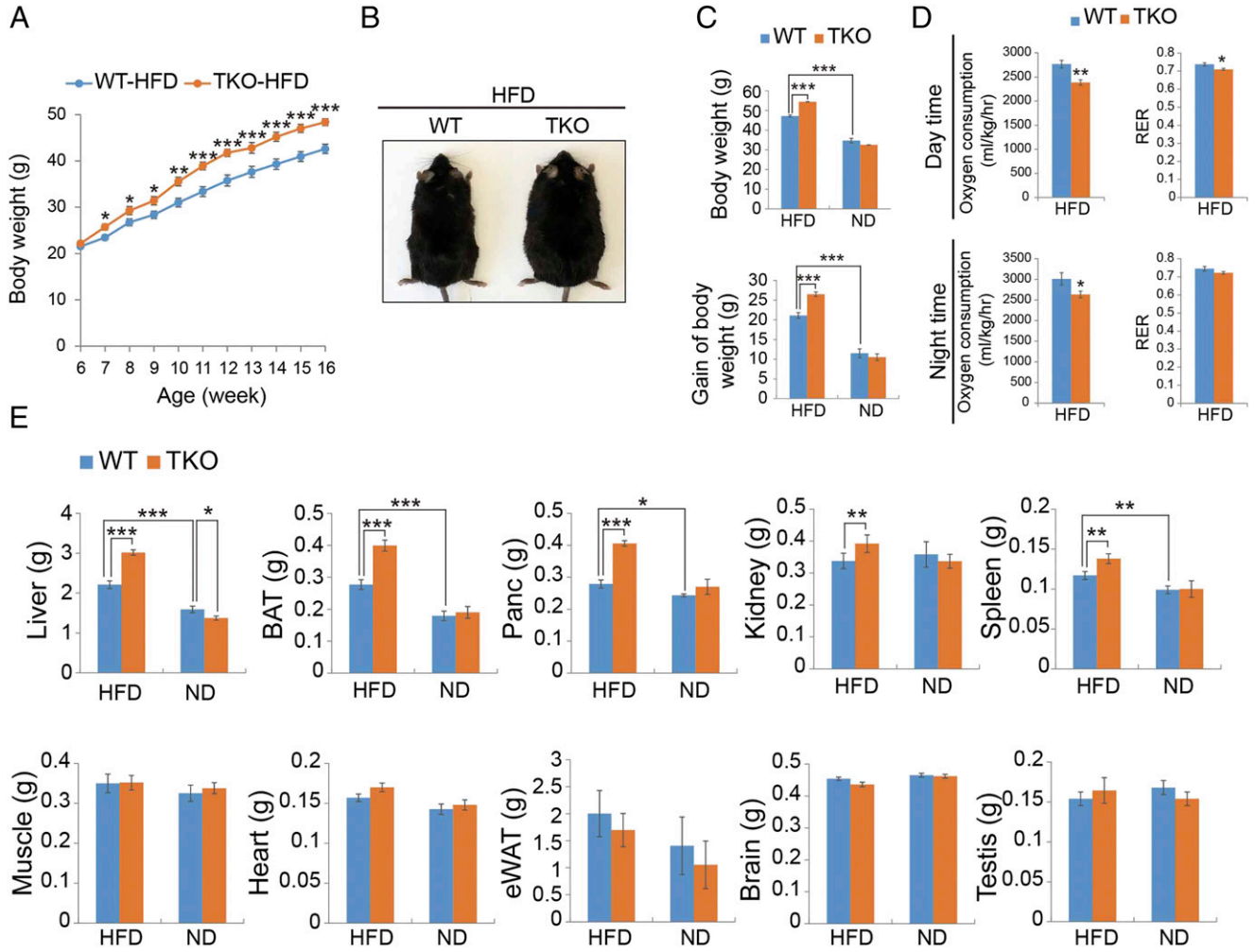

FIGURE 2. Lack of 4E-BPs promotes obesity in response to an HFD. (**A**) Weekly body weight measurements of WT and TKO mice on an HFD. (**B**) Representative image of WT and 4E-BP1/2/3 TKO mice fed an HFD at 16 wk.(**C**) Body weight and gain of body weight measurements of WT and TKO mice fed a normal diet or HFD at 16 wk. (**D**) Measurement of oxygen consumption and RER in WT and TKO mice fed an HFD. The RER measured by the volume of CO_2 produced divided by the volume of O_2 consumed. (**E**) Tissue weights of WT and TKO mice fed a normal diet or HFD at 16 wk. Data are mean ± SEM (n = 10). Using two-way ANOVA with Bonferroni post hoc test. *$p < 0.05$, **$p < 0.01$, ***$p < 0.001$. ND, normal diet.

obesity-related complications (30–34). We therefore examined the expression of three additional IRFs (IRF1, IRF3, and IRF5), which have been implicated in Mϕ polarization in adipose tissue (30, 31, 33). Whereas the levels of IRF3 and IRF5 were not different between WT and TKO mice (Fig. 3F, 3G, respectively), IRF1 expression was significantly induced at the protein level in TKO mice in response to HFD (fold change: 2.8 TKO versus WT) (Fig. 3F). Unlike IRF8, we did not detect significant difference in IRF1 expressions between TKO and WT BMDMs in response to LPS/IFN-γ treatment (Supplemental Fig. 4C, right panel). Given the strong induction of IRF8 in both TKO BMDMs and TKO eWAT Mϕs, we reason that the inflammatory phenotype of eWAT Mϕs in response to HFD and BMDMs in response to LPS/IFN-γ rely on IRF8 activity.

4E-BPs control the translation of Irf8 *mRNA*

To directly demonstrate that *Irf8* mRNAs' translation is controlled by 4E-BPs, we performed polysome-profiling analysis on livers from WT and TKO mice (Fig. 4). We used liver because we could not collect a sufficient number of Mϕs from adipose tissue. It is noteworthy that, in response to HFD, a higher percentage of F4/80$^+$ Mϕs was observed in the TKO livers compared with WT livers (Supplemental Fig. 4E) (35). We observed an increase in the polysome to 80S ratio in the TKO HFD livers compared with WT HFD livers, indicating an increase in translation in TKO livers in response to HFD (Fig. 4A). In contrast, we did not detect a difference in translation between the livers of normal diet–fed WT and TKO mice (Fig. 4A). We examined the expression of IRF1, IRF3, IRF5, and IRF8 in liver samples from WT and TKO mice fed with ND or HFD. In agreement with the eWAT data, protein levels of IRF8 were increased in the liver of TKO mice fed an HFD as compared with their WT counterparts (Supplemental Fig. 4F–H). Although the levels of IRF1, IRF3, and IRF5 appeared to be higher in HFD TKO livers compared with WT samples, differences were not statistically significant (Supplemental Fig. 4F–H). RT-qPCR analysis of the polysome fractions showed that *Irf1*, *Irf3*, and *Irf8* mRNAs sedimented with heavier polysome fractions in TKO HFD livers as compared with the WT HFD livers (Fig. 4B), indicating augmented translation. Whereas IRF8 play critical roles in proinflammatory activation of Mϕs, IRF3 has been linked to anti-inflammatory responses (36). In addition, unlike IRF8, we did not detect a significant difference in IRF3 levels in HFD TKO eWAT compared with HFD WT eWAT. Thus, we conclude that the lack of 4E-BPs

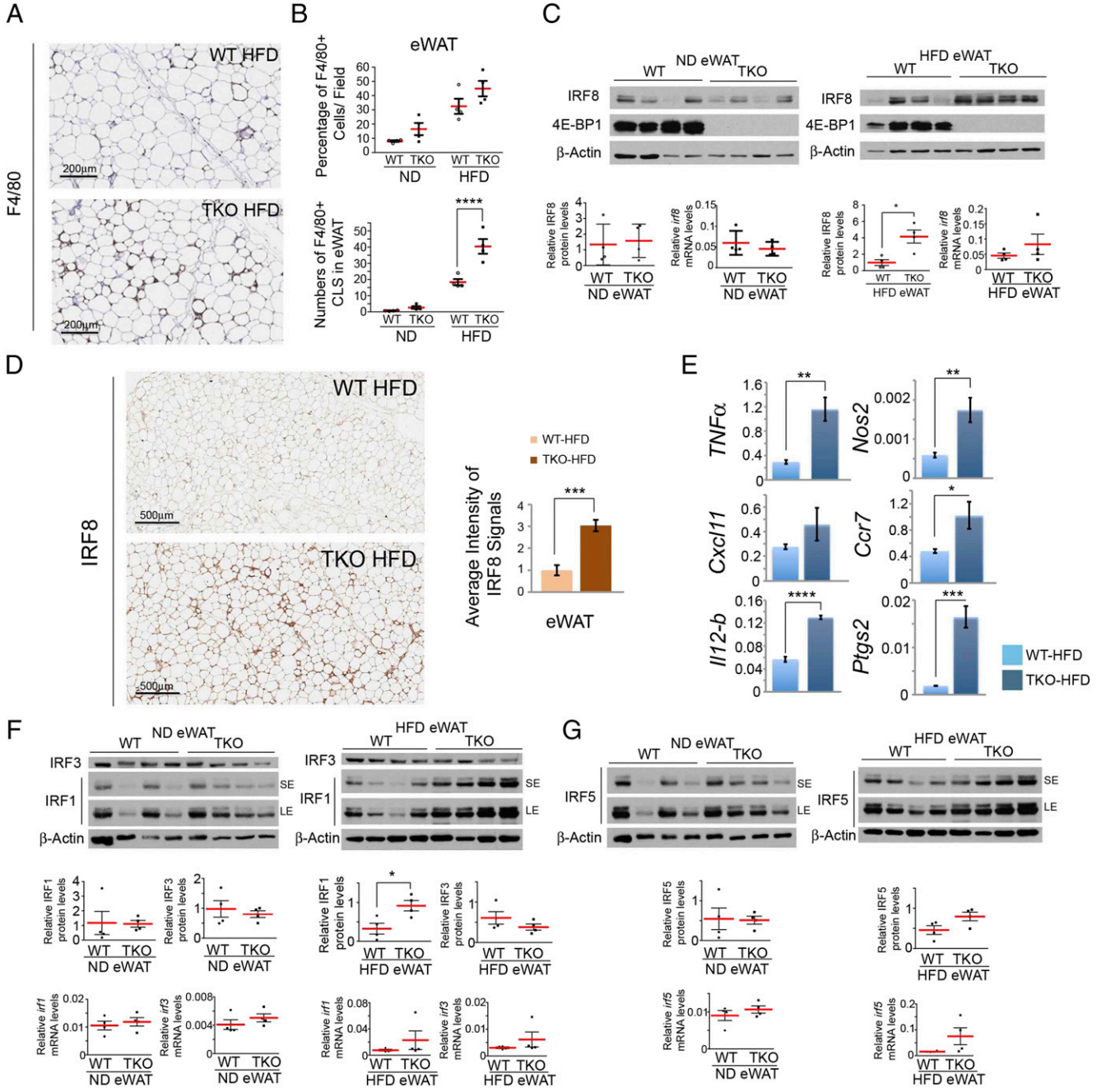

FIGURE 3. Lack of 4E-BPs promotes proinflammatory polarization of adipose tissue Mϕs and IRF1 and IRF8 expression in response to an HFD. (**A**) Representative images of F4/80 IHC of WT and TKO HFD eWAT (positive cells stained brown). Scale bars, 200 μm. (**B**) Quantification of F4/80$^+$ cells and F4/80$^+$ CLS in eWAT sections by taking the average of five randomly selected microscopic fields per mouse. Data are mean ± SEM ($n = 4$). ****$p < 0.0001$, two-way ANOVA with Bonferroni post hoc test. (**C**) Western blot analysis of IRF8, quantification of IRF8 (normalized to β-actin), and corresponding mRNA levels in WT and TKO eWAT of mice fed a normal diet or HFD. The mRNA levels are normalized to *Hprt*. Data are mean ± SEM ($n = 4$). *$p < 0.05$, unpaired Student t test. (**D**) Representative images and quantification of IRF8 IHC of WT and TKO HFD eWAT. Data are mean ± SD ($n = 3$). Scale bars, 500 μm. (**E**) RT-qPCR analysis ($n = 3$) of indicated mRNAs in F4/80$^+$Cd11b$^+$ eWAT Mϕs obtained from HFD-fed WT and TKO mice. (**F** and **G**) Western blot analysis of IRFs, quantification of IRFs (normalized to β-Actin), and corresponding mRNA levels in WT and TKO eWAT of mice fed a normal diet or HFD. Short exposure (SE) and long exposure (LE). Using unpaired Student t test. *$p < 0.05$, **$p < 0.01$, ***$p < 0.001$, ****$p < 0.0001$. ND, normal diet.

promotes inflammatory Mϕ responses through increased translation of *Irf8* (Fig. 4C).

Discussion

In this study, we demonstrated that 4E-BP1/2/3 TKO BMDMs polarized better than WT to inflammatory Mϕs (Fig. 1, Supplemental Fig. 2D–G). We used an HFD-induced obesity mouse model to explore the role 4E-BPs in Mϕ polarization in vivo. TKO mice gained more weight in response to an HFD compared with WT animals (Fig. 2A–C). This finding is consistent with a previous study showing that 4E-BP1/2 DKO mice are more sensitive to diet-induced obesity (12). Le Bacquer et al. attributed the increased sensitivity of 4E-BP1/2 DKO mice to HFD to higher expression of C/EBδ, C/EBPα, and PPAR-γ combined with reduced metabolic rate (decreased in oxygen consumption). Measurement of oxygen consumption rate and the RER of HFD-fed TKO mice also

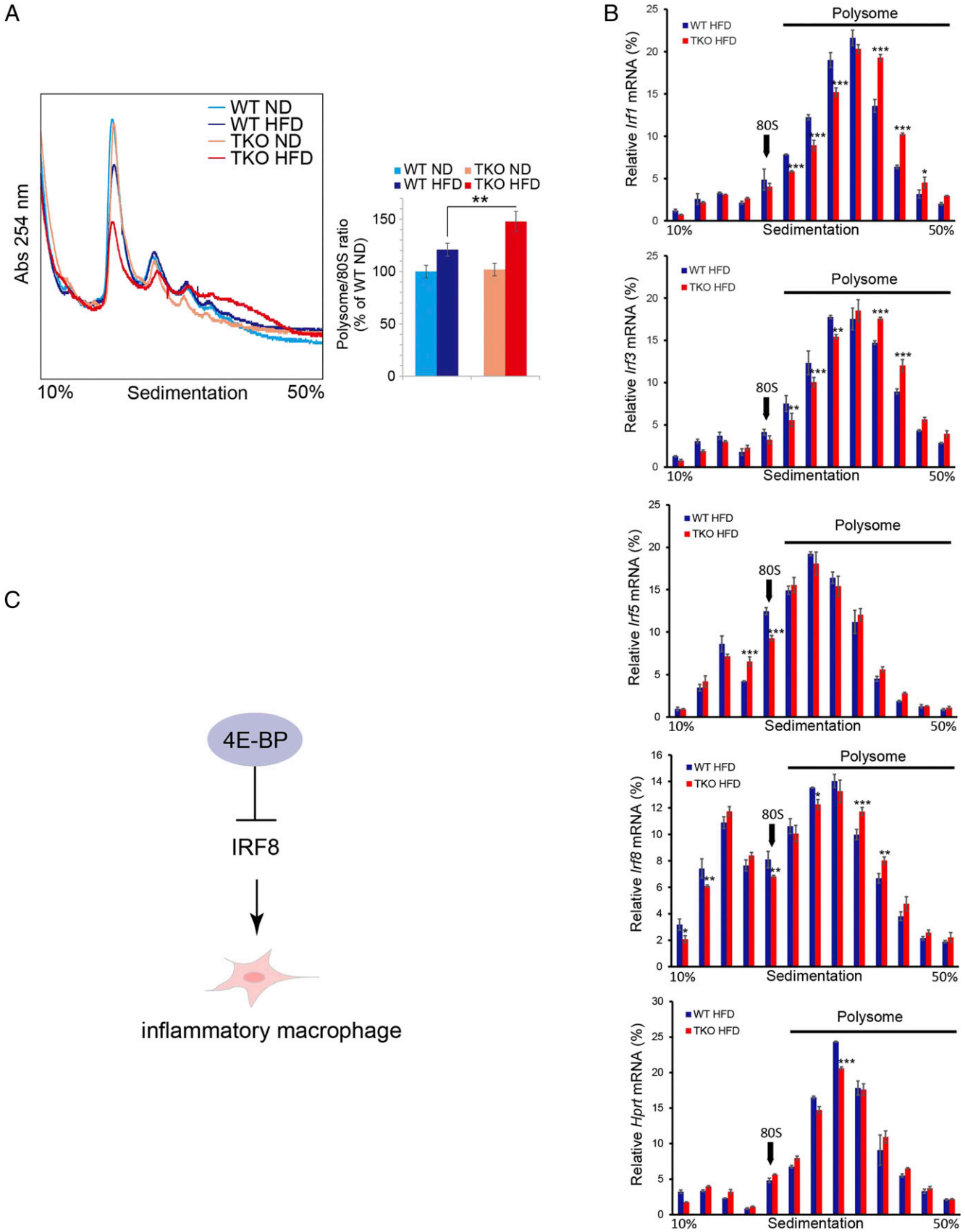

FIGURE 4. 4E-BP–dependent translational control of *Irfs*. (**A**) Representative polysome profiles of WT and TKO livers of mice fed a normal diet or HFD and quantification of polysome to 80S ratio as determined by area under the curve ($n = 6$). (**B**) RT-qPCR analysis of *Irf1, 3, 5*, and *8* mRNAs in WT and TKO HFD liver polysome fractions. *Hprt* mRNA was used as a negative control. Data represent mean ± SD. A representative experiment of two independent experiments (each carried out in triplicate) is presented. (**C**) Model showing the regulation of inflammatory Mϕs by 4E-BPs. Lack of 4E-BPs promotes *Irf8* mRNA translations that causes an increase in inflammatory response in Mϕs. Two-way ANOVA with Bonferroni post hoc test. $*p < 0.05$, $**p < 0.01$, $***p < 0.001$. ND, normal diet.

showed reduced metabolism compared with WT controls (Fig. 2D). Furthermore, HFD induced a pronounced accumulation of inflammatory Mϕs in eWAT of TKO mice and a significant increase in the IRF1 and IRF8 expression and their targets in TKO eWAT (Fig. 3). We also found that a lack of 4E-BPs promotes translation of *Irf1*, *Irf3*, and *Irf8* mRNAs (Fig. 4). A recent study by William et al. (20) reported that the proinflammatory chemokines CCL5 and CXL10 are subjected to translational control by 4E-BPs in Mϕs. Extending these findings, our data reveal a new facet to the role of 4E-BP–dependent translational control in inflammatory response through regulation of IRF8 expression.

IRF8, also known as IFN consensus sequence binding protein (ICSBP), belongs to the IRF family. IRFs control the expression of type I IFN–stimulated genes via binding to IFN-stimulated responsive elements. IRF8 has a critical role in the regulation of myeloid-specific hematopoietic differentiation toward Mϕ lineages and in the maturation and activation of Mϕs (37, 38). Accordingly, *Irf8* mutations occur in a subset of human primary immunodeficiencies (39). In addition to this study, other studies have also provided the link between eIF4E activity and expression of IRF8. Xu et al. (29) demonstrated that eIF4E controls *Irf8* mRNA translation downstream of Notch–RBP-J signaling. In addition, Karmaus et al. (40) showed that activation of mTORC1 in response to M-CSF promotes IRF8 expression in hematopoietic progenitors to enhance myelopoiesis and differentiation of monocyte and Mϕ. Although it is not known whether M-CSF–mediated activation of mTORC1 promotes IRF8 expression at the transcription or translation levels in hematopoietic progenitors, it is highly likely that 4E-BP–dependent translational control of *Irf8* downstream of mTORC1 contributes to mTOR-dependent myelopoiesis. In addition to IRF8, we showed that IRF1 amounts are increased in TKO eWAT in response to HFD, and 4E-BPs control translation of *Irf1* mRNA (Fig. 4B). IRF8 and IRF1 interact with each other (41) and coregulate expression of the genes involved in Mϕ activation and proinflammatory responses (21, 42, 43). IRF8 may exert its proinflammatory effects on TKO Mϕs in cooperation with IRF1. Given the lack of a difference in levels of IRF1 between WT and TKO BMDMs in response to LPS/IFN-γ (Supplemental Fig. 4C, right panel) we did not further assess this potential cooperation by combined IRF1 and IRF8 knockdown. Future work is required to understand the contribution of other IRFs in proinflammatory phenotypes of TKO mice. The novel role of the 4E-BP–IRF8 axis in proinflammatory Mϕ polarization (Fig. 4C) provides insight into how translation engenders tissue resident Mϕs to respond to environmental cues in both homeostatic and pathological states, such as obesity.

Lastly, although our data point to Mϕs as the key cell type mediating the effect of 4E-BPs in inflammatory responses of HFD-fed mice, conditional myeloid cell 4E-BP knockout mice and bone marrow transplantation experiments are required to ultimately prove our model. In addition, recent studies have highlighted the importance of the host microbiome and the large impact it may have on the phenotypes observed in mice (44). This is particularly a concern when studying inflammatory-associated phenotypes, such as our study. As described in the *Materials and Methods*, our mice have been kept together in the same room and the same rack and have experienced the same environmental factors that may impact the microbiome. However, we cannot rule out the impact of cage or genotype on microbiome.

Disclosures

The authors have no financial conflicts of interest.

References

1. Piccirillo, C. A., E. Bjur, I. Topisirovic, N. Sonenberg, and O. Larsson. 2014. Translational control of immune responses: from transcripts to translatomes. *Nat. Immunol.* 15: 503–511.
2. Jovanovic, M., M. S. Rooney, P. Mertins, D. Przybylski, N. Chevrier, R. Satija, E. H. Rodriguez, A. P. Fields, S. Schwartz, R. Raychowdhury, et al. 2015. Immunogenetics. Dynamic profiling of the protein life cycle in response to pathogens. *Science* 347: 1259038.
3. Liu, Y., A. Beyer, and R. Aebersold. 2016. On the dependency of cellular protein levels on mRNA abundance. *Cell* 165: 535–550.
4. Hinnebusch, A. G., I. P. Ivanov, and N. Sonenberg. 2016. Translational control by 5′-untranslated regions of eukaryotic mRNAs. *Science* 352: 1413–1416.
5. Pause, A., G. J. Belsham, A.-C. Gingras, O. Donzé, T. A. Lin, J. C. Lawrence, Jr., and N. Sonenberg. 1994. Insulin-dependent stimulation of protein synthesis by phosphorylation of a regulator of 5′-cap function. *Nature* 371: 762–767.
6. Gingras, A. C., B. Raught, S. P. Gygi, A. Niedzwiecka, M. Miron, S. K. Burley, R. D. Polakiewicz, A. Wyslouch-Cieszynska, R. Aebersold, and N. Sonenberg. 2001. Hierarchical phosphorylation of the translation inhibitor 4E-BP1. *Genes Dev.* 15: 2852–2864.
7. Colina, R., M. Costa-Mattioli, R. J. Dowling, M. Jaramillo, L. H. Tai, C. J. Breitbach, Y. Martineau, O. Larsson, L. Rong, Y. V. Svitkin, et al. 2008. Translational control of the innate immune response through IRF-7. *Nature* 452: 323–328.
8. Jaramillo, M., M. A. Gomez, O. Larsson, M. T. Shio, I. Topisirovic, I. Contreras, R. Luxenburg, A. Rosenfeld, R. Colina, R. W. McMaster, et al. 2011. *Leishmania* repression of host translation through mTOR cleavage is required for parasite survival and infection. *Cell Host Microbe* 9: 331–341.
9. Teleman, A. A., Y. W. Chen, and S. M. Cohen. 2005. 4E-BP functions as a metabolic brake used under stress conditions but not during normal growth. *Genes Dev.* 19: 1844–1848.
10. Tsukiyama-Kohara, K., F. Poulin, M. Kohara, C. T. DeMaria, A. Cheng, Z. Wu, A. C. Gingras, A. Katsume, M. Elchebly, B. M. Spiegelman, et al. 2001. Adipose tissue reduction in mice lacking the translational inhibitor 4E-BP1. *Nat. Med.* 7: 1128–1132.
11. Tsukumo, Y., T. Alain, B. D. Fonseca, R. Nadon, and N. Sonenberg. 2016. Translation control during prolonged mTORC1 inhibition mediated by 4E-BP3. *Nat. Commun.* 7: 11776.
12. Le Bacquer, O., E. Petroulakis, S. Paglialunga, F. Poulin, D. Richard, K. Cianflone, and N. Sonenberg. 2007. Elevated sensitivity to diet-induced obesity and insulin resistance in mice lacking 4E-BP1 and 4E-BP2. *J. Clin. Invest.* 117: 387–396.
13. Le Bacquer, O., K. Combe, C. Montaurier, J. Salles, C. Giraudet, V. Patrac, C. Domingues-Faria, C. Guillet, K. Louche, Y. Boirie, et al. 2017. Muscle metabolic alterations induced by genetic ablation of 4E-BP1 and 4E-BP2 in response to diet-induced obesity. *Mol. Nutr. Food Res.* DOI: 10.1002/mnfr.201700128.
14. Tsai, S., J. M. Sitzmann, S. G. Dastidar, A. A. Rodriguez, S. L. Vu, C. E. McDonald, E. C. Academia, M. N. O'Leary, T. D. Ashe, A. R. La Spada, and B. K. Kennedy. 2015. Muscle-specific 4E-BP1 signaling activation improves metabolic parameters during aging and obesity. *J. Clin. Invest.* 125: 2952–2964.
15. Davies, L. C., S. J. Jenkins, J. E. Allen, and P. R. Taylor. 2013. Tissue-resident macrophages. *Nat. Immunol.* 14: 986–995.
16. Mowat, A. M., C. L. Scott, and C. C. Bain. 2017. Barrier-tissue macrophages: functional adaptation to environmental challenges. *Nat. Med.* 23: 1258–1270.
17. Mills, C. D., K. Kincaid, J. M. Alt, M. J. Heilman, and A. M. Hill. 2000. M-1/M-2 macrophages and the Th1/Th2 paradigm. *J. Immunol.* 164: 6166–6173.
18. Lumeng, C. N., J. L. Bodzin, and A. R. Saltiel. 2007. Obesity induces a phenotypic switch in adipose tissue macrophage polarization. *J. Clin. Invest.* 117: 175–184.
19. William, M., L. P. Leroux, V. Chaparro, J. Lorent, T. E. Graber, M. N. M'Boutchou, T. Charpentier, A. Fabié, C. M. Dozois, S. Stäger, et al. 2018. eIF4E-binding proteins 1 and 2 limit macrophage anti-inflammatory responses through translational repression of IL-10 and cyclooxygenase-2. *J. Immunol.* 200: 4102–4116.
20. William, M., L. P. Leroux, V. Chaparro, T. E. Graber, T. Alain, and M. Jaramillo. 2019. Translational repression of Ccl5 and Cxcl10 by 4E-BP1 and 4E-BP2 restrains the ability of mouse macrophages to induce migration of activated T cells. *Eur. J. Immunol.* 49: 1200–1212.
21. Langlais, D., L. B. Barreiro, and P. Gros. 2016. The macrophage IRF8/IRF1 regulome is required for protection against infections and is associated with chronic inflammation. *J. Exp. Med.* 213: 585–603.
22. Tahmasebi, S., S. M. Jafarnejad, I. S. Tam, T. Gonatopoulos-Pournatzis, E. Matta-Camacho, Y. Tsukumo, A. Yanagiya, W. Li, Y. Atlasi, M. Caron, et al. 2016. Control of embryonic stem cell self-renewal and differentiation via coordinated alternative splicing and translation of YY2. *Proc. Natl. Acad. Sci. USA* 113: 12360–12367.
23. Morita, M., T. Alain, I. Topisirovic, and N. Sonenberg. 2013. Polysome profiling analysis. *Bio-protocol* 3: 3–8.
24. Byles, V., A. J. Covarrubias, I. Ben-Sahra, D. W. Lamming, D. M. Sabatini, B. D. Manning, and T. Horng. 2013. The TSC-mTOR pathway regulates macrophage polarization. *Nat. Commun.* 4: 2834.
25. Thoreen, C. C., L. Chantranupong, H. R. Keys, T. Wang, N. S. Gray, and D. M. Sabatini. 2012. A unifying model for mTORC1-mediated regulation of mRNA translation. *Nature* 485: 109–113.
26. Cinti, S., G. Mitchell, G. Barbatelli, I. Murano, E. Ceresi, E. Faloia, S. Wang, M. Fortier, A. S. Greenberg, and M. S. Obin. 2005. Adipocyte death defines macrophage localization and function in adipose tissue of obese mice and humans. *J. Lipid Res.* 46: 2347–2355.
27. McLaughlin, T., S. E. Ackerman, L. Shen, and E. Engleman. 2017. Role of innate and adaptive immunity in obesity-associated metabolic disease. *J. Clin. Invest.* 127: 5–13.

28. Lackey, D. E., and J. M. Olefsky. 2016. Regulation of metabolism by the innate immune system. *Nat. Rev. Endocrinol.* 12: 15–28.
29. Xu, H., J. Zhu, S. Smith, J. Foldi, B. Zhao, A. Y. Chung, H. Outtz, J. Kitajewski, C. Shi, S. Weber, et al. 2012. Notch-RBP-J signaling regulates the transcription factor IRF8 to promote inflammatory macrophage polarization. *Nat. Immunol.* 13: 642–650.
30. Friesen, M., R. Camahort, Y. K. Lee, F. Xia, R. E. Gerszten, E. P. Rhee, R. C. Deo, and C. A. Cowan. 2017. Activation of IRF1 in human adipocytes leads to phenotypes associated with metabolic disease. *Stem Cell Rep.* 8: 1164–1173.
31. Kumari, M., X. Wang, L. Lantier, A. Lyubetskaya, J. Eguchi, S. Kang, D. Tenen, H. C. Roh, X. Kong, L. Kazak, et al. 2016. IRF3 promotes adipose inflammation and insulin resistance and represses browning. *J. Clin. Invest.* 126: 2839–2854.
32. Eguchi, J., X. Kong, M. Tenta, X. Wang, S. Kang, and E. D. Rosen. 2013. Interferon regulatory factor 4 regulates obesity-induced inflammation through regulation of adipose tissue macrophage polarization. *Diabetes* 62: 3394–3403.
33. Dalmas, E., A. Toubal, F. Alzaid, K. Blazek, H. L. Eames, K. Lebozec, M. Pini, I. Hainault, E. Montastier, R. G. Denis, et al. 2015. Irf5 deficiency in macrophages promotes beneficial adipose tissue expansion and insulin sensitivity during obesity. *Nat. Med.* 21: 610–618.
34. Wang, X. A., R. Zhang, S. Zhang, S. Deng, D. Jiang, J. Zhong, L. Yang, T. Wang, S. Hong, S. Guo, et al. 2013. Interferon regulatory factor 7 deficiency prevents diet-induced obesity and insulin resistance. *Am. J. Physiol. Endocrinol. Metab.* 305: E485–E495.
35. Morinaga, H., R. Mayoral, J. Heinrichsdorff, O. Osborn, N. Franck, N. Hah, E. Walenta, G. Bandyopadhyay, A. R. Pessentheiner, T. J. Chi, et al. 2015. Characterization of distinct subpopulations of hepatic macrophages in HFD/obese mice. *Diabetes* 64: 1120–1130.
36. Günthner, R., and H. J. Anders. 2013. Interferon-regulatory factors determine macrophage phenotype polarization. *Mediators Inflamm.* 2013: 731023.
37. Chistiakov, D. A., V. A. Myasoedova, V. V. Revin, A. N. Orekhov, and Y. V. Bobryshev. 2018. The impact of interferon-regulatory factors to macrophage differentiation and polarization into M1 and M2. *Immunobiology* 223: 101–111.
38. Zhao, G. N., D. S. Jiang, and H. Li. 2015. Interferon regulatory factors: at the crossroads of immunity, metabolism, and disease. *Biochim. Biophys. Acta* 1852: 365–378.
39. Hambleton, S., S. Salem, J. Bustamante, V. Bigley, S. Boisson-Dupuis, J. Azevedo, A. Fortin, M. Haniffa, L. Ceron-Gutierrez, C. M. Bacon, et al. 2011. IRF8 mutations and human dendritic-cell immunodeficiency. *N. Engl. J. Med.* 365: 127–138.
40. Karmaus, P. W. F., A. A. Herrada, C. Guy, G. Neale, Y. Dhungana, L. Long, P. Vogel, J. Avila, C. B. Clish, and H. Chi. 2017. Critical roles of mTORC1 signaling and metabolic reprogramming for M-CSF-mediated myelopoiesis. *J. Exp. Med.* 214: 2629–2647.
41. Bovolenta, C., P. H. Driggers, M. S. Marks, J. A. Medin, A. D. Politis, S. N. Vogel, D. E. Levy, K. Sakaguchi, E. Appella, J. E. Coligan, et al. 1994. Molecular interactions between interferon consensus sequence binding protein and members of the interferon regulatory factor family. *Proc. Natl. Acad. Sci. USA* 91: 5046–5050.
42. Dror, N., M. Alter-Koltunoff, A. Azriel, N. Amariglio, J. Jacob-Hirsch, S. Zeligson, A. Morgenstern, T. Tamura, H. Hauser, G. Rechavi, et al. 2007. Identification of IRF-8 and IRF-1 target genes in activated macrophages. *Mol. Immunol.* 44: 338–346.
43. Karki, R., E. Lee, D. Place, P. Samir, J. Mavuluri, B. R. Sharma, A. Balakrishnan, R. K. S. Malireddi, R. Geiger, Q. Zhu, et al. 2018. IRF8 regulates transcription of naips for NLRC4 inflammasome activation. *Cell* 173: 920–933.e13.
44. Stappenbeck, T. S., and H. W. Virgin. 2016. Accounting for reciprocal host-microbiome interactions in experimental science. *Nature* 534: 191–199.